Optica Applicata, Vol. XXXIV, No. 3, 2004

Application of the 3-frame interferometry and the crater replica method for investigation of laser accelerated macroparticles interacting with massive targets in the Prague Asterix Laser System (PALS) experiment

STEFAN BORODZIUK[1], ANDRZEJ KASPERCZUK[1], TADEUSZ PISARCZYK[1], NIKOLAY N. DEMCHENKO[2], SERGEY YU. GUS'KOV[2], VLADISLAV B. ROZANOV[2], MILAN KALAL[3], JIRI LIMPOUCH[3, 5], JIRI ULLSCHMIED[4, 5], KAREL ROHLENA[5], JIRI SKALA[5], VLADIMIR N. KONDRASHOV[6], PAWEL PISARCZYK[7]

[1]Institute of Plasma Physics and Laser Microfusion, ul. Hery 23, 00-908 Warszawa, Poland

[2]P.N. Lebedev Physical Institute of RAS, Leninskyi Ave. 53, 117 924 Moscow, Russia

[3]Czech Technical University, FNSPE, Brehova 7, 115 19 Prague 1, Czech Republic

[4]Institute of Plasma Physics, AS CR, Za Slovankou 3, 182 21 Prague 8, Czech Republic

[5]PALS Research Center AS CR, Za Slovankou 3, 182 21 Prague 8, Czech Republic

[6]Troitsk Institute of Innovation and Thermonuclear Research, 142 190 Troitsk, Russia

[7]Warsaw University of Technology, ICS, ul. Nowowiejska 15/19, 00-665 Warszawa, Poland

In the present paper results from our experiments with macroparticles, accelerated at first to high speeds by the PALS iodine laser and subsequently hitting massive targets and creating craters, are presented. The main aim of these investigations concerned the influence of wavelength on the efficiency of macroparticles acceleration and creation of craters. To this end, two different harmonics of the PALS laser beam (λ_1 = 1.315 μm and λ_3 = 0.438 μm) and several types of targets (simple massive planar Al targets as well as much more elaborated double targets consisting of 6 μm thick Al foils or disks placed in front of the massive target at the distance of either 200 μm or 500 μm) were used. All these targets were irradiated by the iodine laser beam with its parameters very much the same for both harmonics: the energy of 130 J, the focal spot diameter of 250 μm, and the pulse duration of 400 ps. Velocities of accelerated extracted foil fragments or disks as well as electron density distributions of plasma streams were determined by means of the 3-frame interferometry. Shapes and volumes of craters were obtained employing the crater acetate cellulose replica technology and microscopy measurements. The data from these experiments provided valuable information concerning the ablative plasma generation and crater creation processes.

Keywords: laser produced plasma, three-frame interferometry, optical microscopy, macroparticle, single and double targets, crater, classical inverse bremsstrahlung absorption, shock wave, efficiency of laser radiation absorption, ablation loading efficiency.

1. Introduction

The laser-planar target experiments play a fundamental role in the study of laser -produced plasma physics and the problems related to inertial confinement fusion (ICF). They represent the starting point for numerous physical phenomena analysis and provide information necessary for research work in the domain of complex configurations such as implosion experiments with spherical targets on which the idea of laser fusion is based.

Experiments utilizing ablatively accelerated planar targets can model large pellet shells in their early implosion phase. Instead of imploding a pellet, a disk target can be accelerated and treated as a section of a sphere (until convergence effects dominate). Another very important problem which can be investigated in planar experiments is the value of initial entropy injected under the laser beam action into the solid part of targets – the key characteristics to find the conditions of high compression of the fuel in ICF. One of the main advantages of experiments with the disk targets lies in the fact that they make the diagnostic of the cold inner surface of spherical targets possible, otherwise rather difficult to access in experiments with the real pellets. The main areas of thin foil experiments are usually the physics of laser-plasma interaction (radiation absorption, heat transport, electron distribution) and ablation acceleration physics (generation of the ablation pressure and the shock wave, hydrodynamic efficiency, energy transfer, Rayleigh–Taylor instability, laser pulse uniformity requirements and so on), *e.g.*, [1]–[3].

Some other applications of the experiments using simple or more complex planar targets, very useful in fusion research, are, *e.g.*, the possibility of extremely high pressure generation and ablative acceleration of very fast macroparticles. Such fast macroparticle is one of the most effective types of igniting drivers [4] for the fast ignition approach [5], [6] in ICF.

When thin foil accelerated by means of the laser beam to reach velocity of more than 10^7 cm/s collides with the target at rest, a very strong shock wave and a pressure of 100 Mbar can be generated.

The craters created by the accelerated foil can provide some very useful data explaining many features of interest.

The two main aims of our investigation were determination of the macroparticles acceleration and craters creation efficiency depending on:

– origin of macroparticles (an extracted foil fragment or prefabricated disk),

– wavelength of the laser beam.

In the first case, our natural expectation was that, contrary to the extracted foil fragment variant, the prefabricated disk attached to a mylar foil can be accelerated with negligible energy loss required for its extraction and practically no lateral heat conduction loss.

The second aim was connected with a significant influence of incident radiation wave length on the efficiency of laser light absorption, parameters of evaporated

plasma and, as a consequence, on the energy of macroparticles. Moreover, different laser radiation wavelengths under certain conditions can prove the dominant role of physically different mechanisms of laser radiation absorption. Indeed, at the laser intensity, for example, 5×10^{15} W/cm^2 , the value of $I\lambda^2$ can be changed about one order of magnitude due to a change of the wavelength from $\lambda_1 = 1.315$ μm to $\lambda_3 = 0.438$ μm (i.e., from $I\lambda_1^2 = 9\times10^{15}$ Wμm^2/cm^2 to $I\lambda_3^2 = 10^{15}$ Wμm^2/cm^2). The smaller value of $I\lambda^2$ corresponds to a domination of the classical inverse bremsstrahlung absorption mechanism of laser radiation, while in the case of $I\lambda^2$ W 10^{15} Wμm^2/cm^2 the resonance absorption mechanism plays the dominant role (with the fast electrons responsible for the absorbed laser energy transfer into the target [7], [8]). The main goal of this experiment was to study physical processes connected with irradiation of double targets. For this reason, complex targets irradiated by the laser intensity corresponding to classical inverse bremsstrahlung absorption mechanism ($I = 0.66\times10^{15}$ W/cm^2) were investigated. Nevertheless, the investigation of crater creation under the action of sufficiently high laser intensity at the different wavelengths allows us, in principle, to study an influence of the resonant absorption and the fast electron generation on the parameters of laser-produced plasma [9].

2. Experimental set-up

The experiment was carried out with the use of the PALS iodine laser facility [10]. The laser system, together with the 3-frame interferometry set-up, is shown schematically in Fig. 1. Plasma was generated by the laser beam with its diameter at the vacuum chamber entrance window about 290 mm focused by means of an aspherical lens with focal lengths of 627 mm and 600 mm for the first and the third harmonic, respectively. Targets were irradiated by the iodine laser beam: $E_L = 130$ J for both harmonics, the focal spot diameter of 250 μm, and the pulse duration of 400 ps.

The choice of 130 J of the laser energy for both harmonics was partially influenced by the third harmonic laser energy limitation (the maximum energy available in the third harmonic was about 180 J). On the other hand, however, it was found that the laser energy over certain threshold can result in overheating of macroparticles (particularly disks due to their limited volume) thus leading to their disintegration before an impact. The selected laser energy seemed to be safe enough for both the foils and the disks with thickness of 6 μm.

To study the plasma expansion and macroparticle acceleration, a 3-frame interferometric system with automatic image processing was used. The diagnostic system was illuminated by the third harmonic of the iodine laser. Due to mechanical constrains, the minimum delay between subsequent frames could not be shorter than 3 ns. The time instant of 0 ns corresponds to the maximum of heating laser pulse.

In these experiments several different types of targets (simple massive planar Al targets as well as much more elaborated double targets consisting of 6 μm thick Al

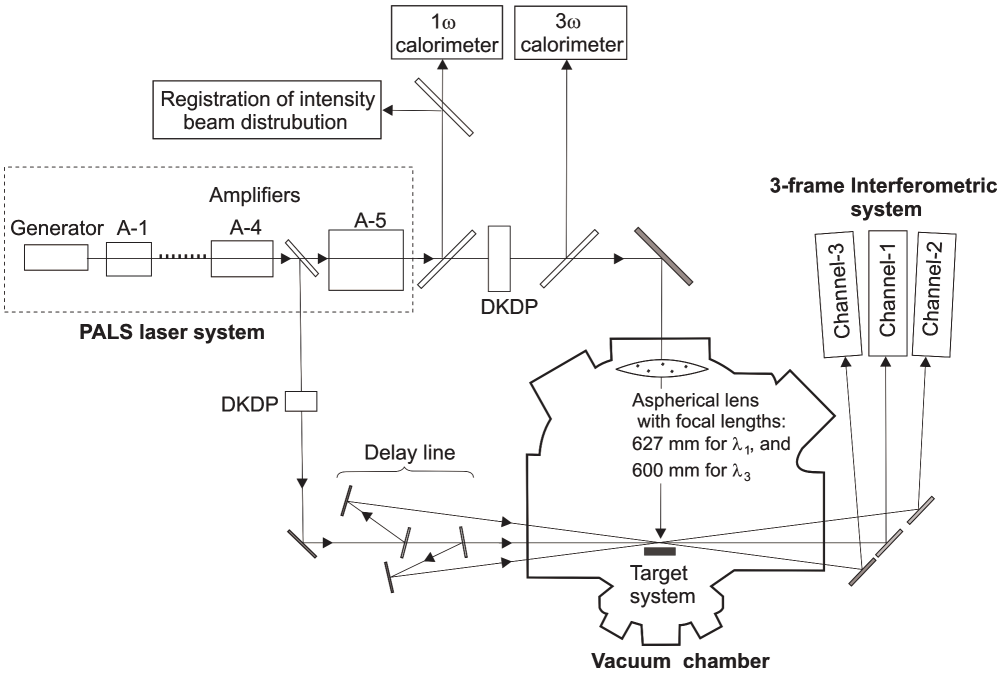

Fig. 1. Experimental set-up.

foils or disks placed in front of the massive target at the distance of either 200 μm or 500 μm) were used. Double targets with the gap of 500 μm were used for the accelerated macroparticle velocity determination (this gap was large enough for registration of two subsequent frames during the macroparticle flight). However, from the point of view of the crater creation itself, such a long distance seemed to be rather unprofitable due to the possibility of accelerated (and heated) macroparticle premature disintegration. Thus, for this purpose a shorter distance of 200 μm was set.

The constructions of the double targets used are presented in Fig. 2. Disks were attached to a supporting mylar foil on the side opposite to the incoming laser beam. To keep the same conditions of the target heating as in the disk case, the front side of all the remaining double targets was covered by the same mylar foil with thickness of 2.5 μm. The target type shown in Fig. 2**b** was used for the crater creation, while the type in Fig. 2**c** served for the disk velocity measurement. Shielding of the disk by the Al foil with a hole a bit smaller than the disk area prevented heating and acceleration of the mylar foil itself. Otherwise, the mylar foil, heated by even a very weak laser radiation falling outside of the disk, would undergo its own acceleration to velocities much higher than 10^7 cm/s, thus screening the disk (the motion of which is considerably slower) from observation. For the crater creation by the disk, however, the double targets without the shielding Al foil were used as the edge of the hole in the covering foil was also heated and its fragments would participate in the crater creation.

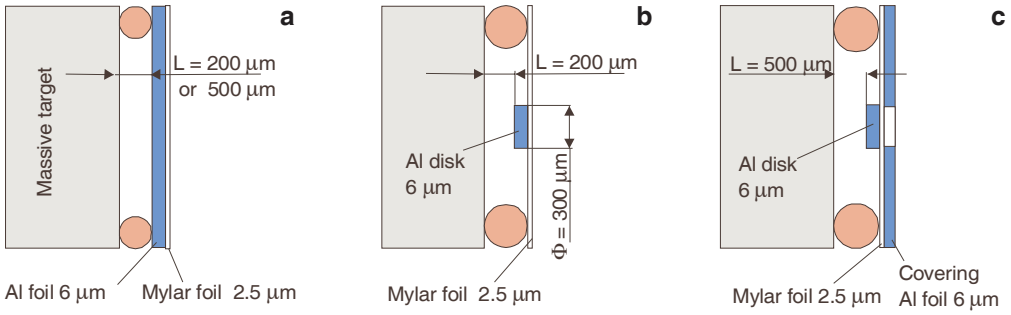

Fig. 2. Constructions of the double targets: foil and massive target (**a**), disk and massive target (**b**), and covered disk and massive target (**c**).

To irradiate the area of the disk as completely as possible (simultaneously avoiding any irradiation of the off-disk region) the focal spot diameter was taken equal to 250 μm (*i.e.*, slightly smaller than the disk diameter). Such irradiation scheme was applied to all remaining targets.

3. Results of interferometric measurements

One of the most important problems connected with the crater creation by very fast macroparticles is determination of their velocities at the moment of an impact. Some information about methodology of macroparticles velocity measurement was presented earlier. For the time being, we would like to pay some attention to a particular problem, which appeared during our experiments. It will be discussed on the basis of Fig. 3. As was already mentioned earlier, for macroparticle velocity measurement the distance of 500 μm between the foil (or the disk) and the massive target was taken. It can be seen in Fig. 3**a** that the macroparticles start moving about 1 ns after the laser action. So, to see clearly the macroparticle position after its start in the first frame, we had to delay this frame by 2 ns with respect to the heating beam. This delay and relatively high velocities of macroparticles accelerated by the third harmonic caused, however, that the distance of 500 μm turned out to be not sufficiently long for this velocity measurement (see Fig. 3**b**). Nevertheless, in the case of the third harmonic this measurement allowed us to estimate the velocity of accelerated macroparticles.

Somewhat contrary to our initial expectation, the macroparticle average velocity determined on the basis of several interferometric sequences seems to be approximately the same for both types of the double targets. This velocity for the first harmonic is equal to $(6 \pm 0.2)\times10^6$ cm/s. In the case of the third harmonic, however, the situation is a bit more complex. The sequence of interferograms in Fig. 3**b** shows that the macroparticle in the period of 3 ns can travel a distance of 400–500 μm. Thus we can conclude that the macroparticle velocity amounts to $(1.3–1.7)\times10^7$ cm/s. Although, even if our velocity measurement is not absolutely precise, it clearly shows that under

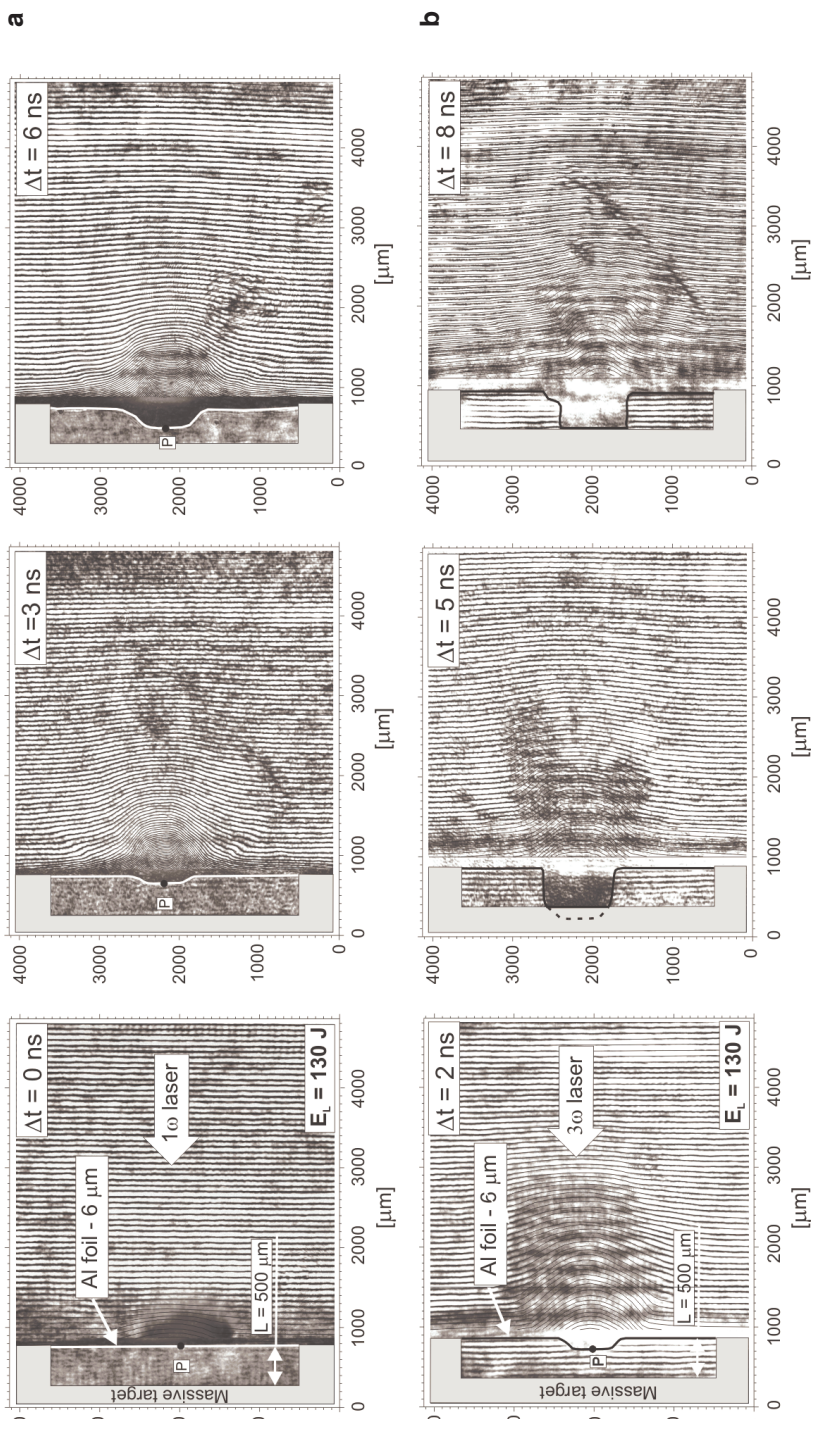

Fig. 3. Two sequences of interferograms showing the ablative plasma expansion and the foil motion for the first harmonic (**a**) and the third harmonic (**b**).

the same irradiation conditions the velocity of macroparticles for the third harmonic is 2.1–2.7 times greater than that for the first harmonic.

To determine the electron density distribution on the basis of the phase shift one, the special numerical methods have been prepared [11]. In the case of axial symmetry of the plasma, the relation between the phase of probing radiation and the electron density in a selected cross-section z of the plasma is expressed by the well-known Abel integral equation:

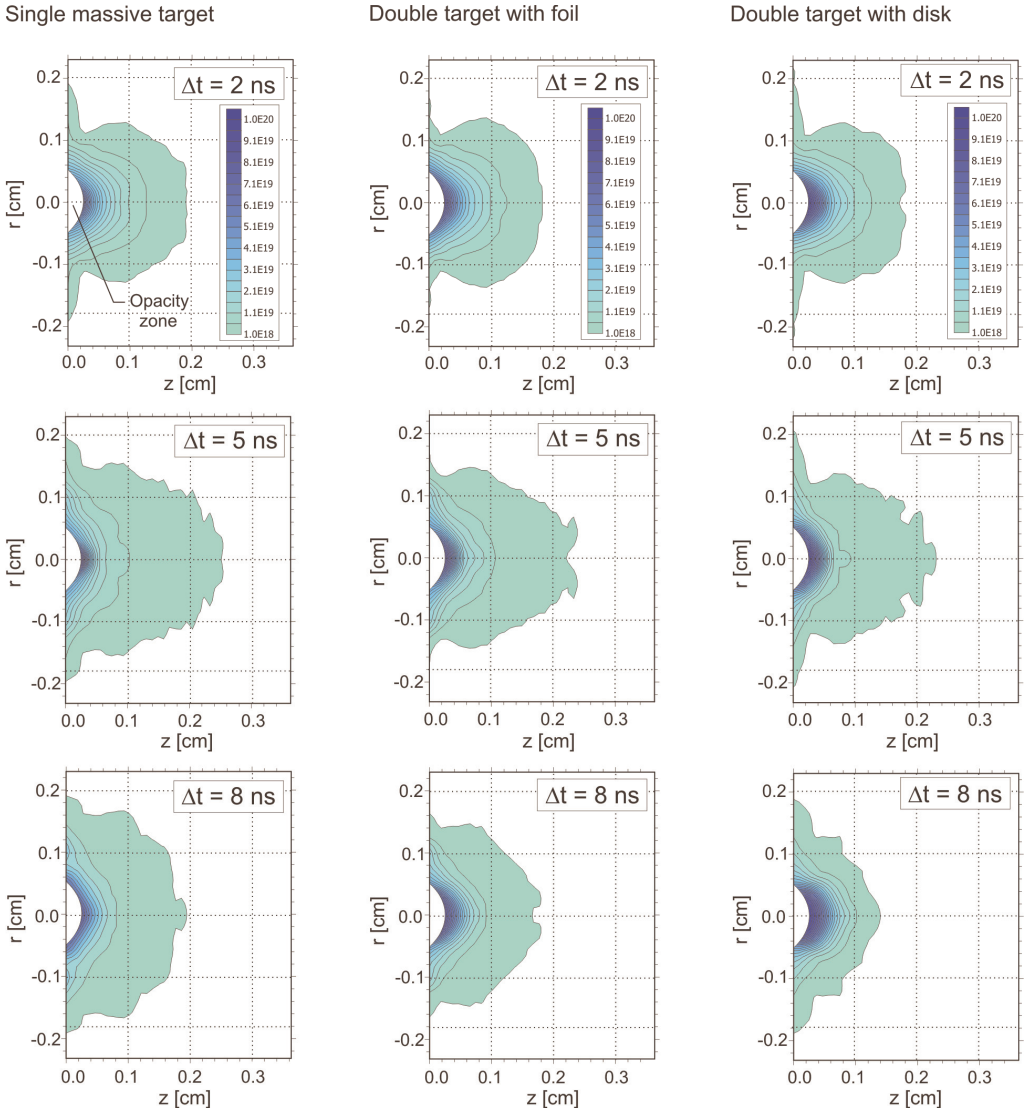

Fig. 4. Sequences of the electron density isodensitograms for the first harmonic of the laser radiation and the three types of the targets: single massive target, double target with foil, and double target with disk. The white fields in the vicinity of the target surface mean the opacity zones.

$$S(y) = 2\int_{y}^{1} \frac{f(r)r}{\sqrt{r^2 - y^2}}\,\mathrm{d}r \tag{1}$$

where: $S(y)$ – the phase distribution [rad/2π], y and r – the coordinates corresponding to one another in an interferogram plane and a real plasma cross-section, respectively,

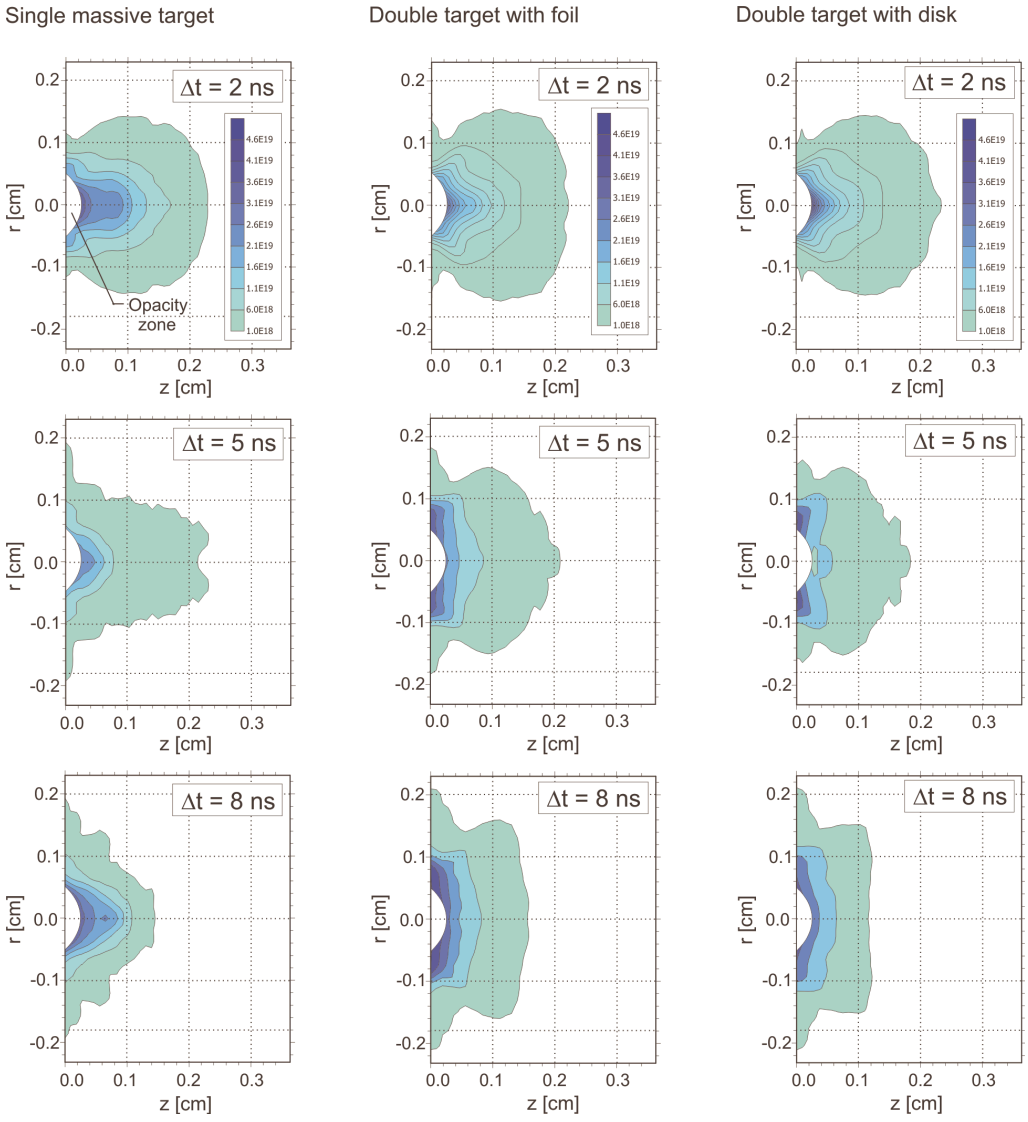

Fig. 5. Sequences of the electron density isodensitograms for the third harmonic of the laser radiation and the three types of the targets: single massive target, double target with foil, and double target with disk. The white fields in the vicinity of the target surface mean the opacity zones.

$f(r) = 4.46\times10^{-14}\lambda R n_e(r)$, while $n_e(r)$ – electron density distribution [cm^{-3}], λ – wavelength of laser radiation [cm], R – radius of plasma for the selected cross-section [cm].

Calculation of the $n_e(r)$ in many cross-sections along the axis "z" allows the full electron density distribution $n_e(r, z)$ to be reconstructed, which can be presented in different graphical forms.

Since the macroparticle acceleration results from plasma ablation, the interferometric investigation of electron density distributions during the early stage of its expansion can provide some interesting information about the ablation and acceleration processes.

In Figures 4 and 5 the sequences of the electron density distributions in the form of isodensitograms at different moments of plasma expansion for all of the tested target types irradiated by the two wavelengths are shown. The plasma stream boundary is represented here by the electron density contour $n_e = 1\times10^{18}$ cm^{-3}. Information about the changes of number of electrons in interesting regions of the plasma stream could be provided by the diagrams of the linear electron density corresponding to these electron density distributions, presented in Fig. 6.

On the basis of the interferometric measurements we have obtained the following information.

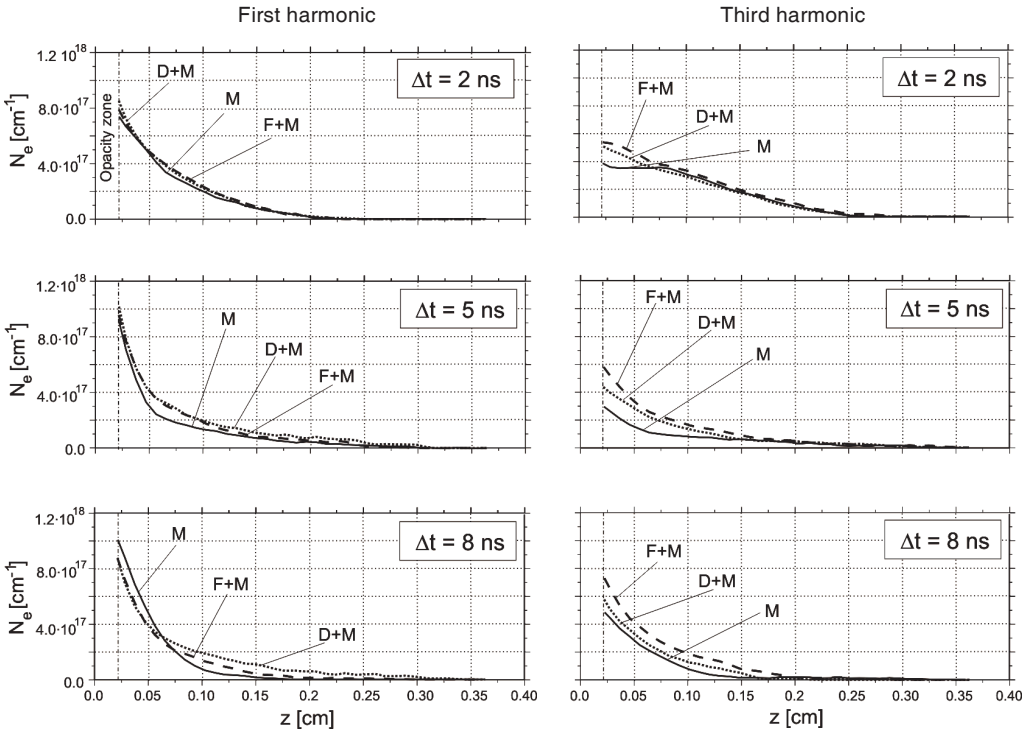

Fig. 6. Linear electron density distributions for the tested targets: M – single massive target, M+F – double target with foil, and M+D – double target with disk as well as for the first harmonic and the third harmonic at different moments of plasma expansion.

The first harmonic. At $\Delta t = 2$ ns the distribution of $n_e(r, z)$ and diagrams of $N_e(z)$ are nearly identical for all the types of the targets. Some differences are only seen at the later moment ($\Delta t = 8$ ns) and particularly concern:

– the size of thin plasma clouds,

– the growth of n_e and N_e in the vicinity of the massive target.

This means, that in the later period the differences in the targets construction play more important role.

The third harmonic. Differences in $n_e(r, z)$ for the different types of the targets are already seen at the moment of 2 ns. While the outer shapes of the plasma streams are similar in all the cases, forms of the dense plasma outflows for the single massive target and the double targets differ considerably. In the case of a single massive target this outflow is elongated along the axis, meanwhile in the other cases the axial plasma stream is shorter and is additionally equipped with a plasma ring located close to the target (seen in the form of wings in the electron density distributions).

In the subsequent period the differences between the single target and the double ones grow and concern both the thin plasma (*i.e.*, size and shape of the plasma stream) and the dense plasma, represented by the inner equidensity lines.

A comparison of the linear electron density diagrams for the two harmonics reveals that the electron number in the region close to the target ($z < 0.05$ cm) is smaller for the case of the third harmonic.

4. Characteristics of craters

In order to obtain information about the shape and dimensions of individual craters, their replicas were made of acetate cellulose. To reconstruct quantitatively the crater shape the crater replica microphotography was taken. Then the crater shape in a chosen cross-section was digitized to be data for further computations.

The created craters as well as their replicas for the targets tested and the two harmonics of the laser radiation are shown in Figs. 7 and 8 (here, R_c and H_c mean the radius and the depth of the craters, respectively). The shapes of the craters from Figs. 7 and 8 are presented in Fig. 9. As some of these shapes deviate substantially from an axial symmetry, they are shown in two mutually perpendicular projections. Based on these shapes the following conclusions can be drawn:

– the craters obtained as a result of a direct laser beam-massive target interaction have approximately a hemispherical shape,

– in the case of double targets, the shapes of craters are similar to each other, but for the first harmonic the craters are shallower and less symmetrical whereas for the third one the crater shapes are close to hemispherical ones.

The essential difference between the first and the third harmonic cases concerns the volumes of craters. Due to the shape irregularity of some craters, their volumes were split into four quarters and the respective volume of each quarter of the crater was established independently. The volumes of the craters presented in Figs. 7–9 are given in the Table.

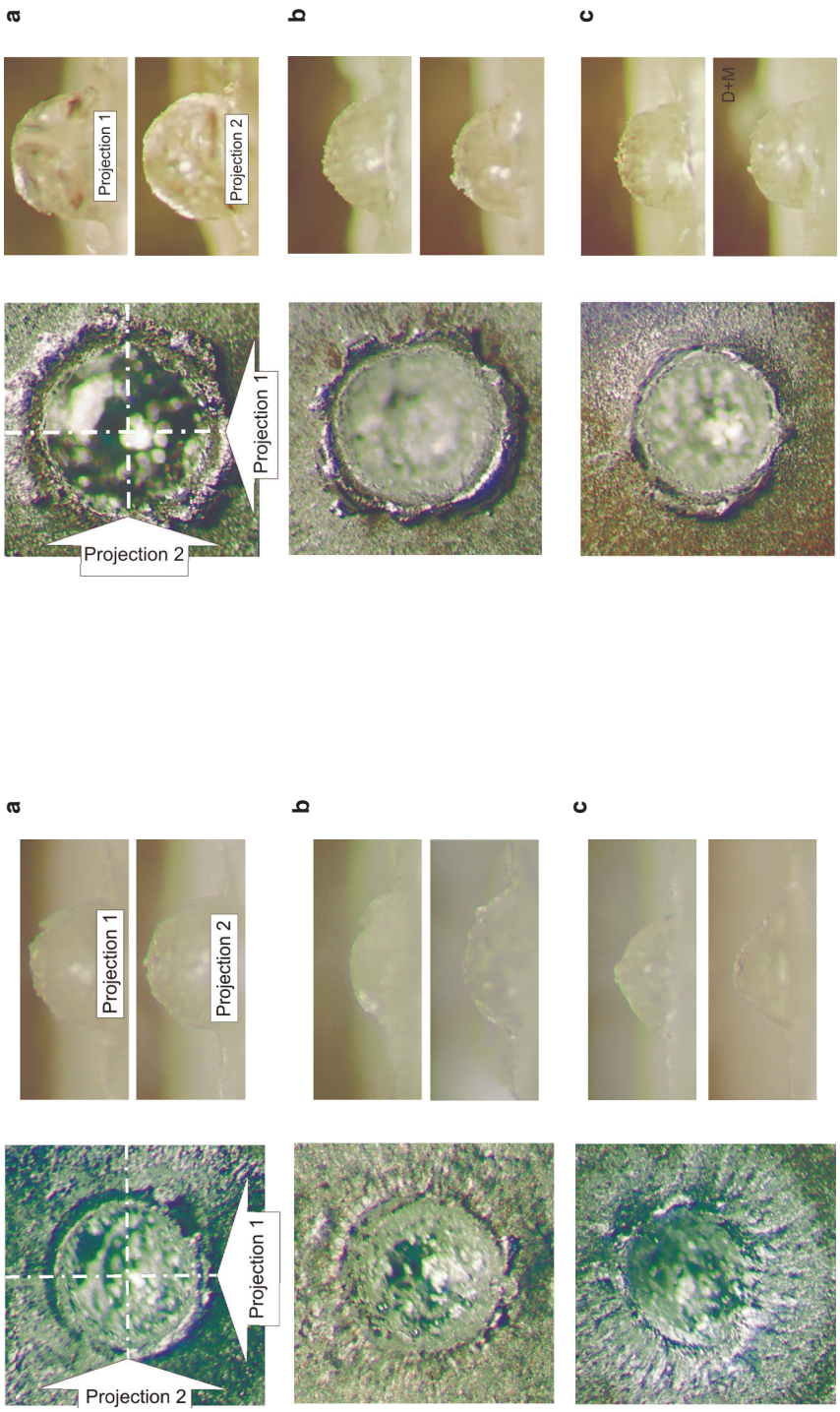

Fig. 7. Craters (left, top view) and crater replicas (right, side view) photographs for the first harmonic of the laser radiation and the three types of the targets: single massive target (**a**), double target with foil (**b**), and double target with disk (**c**).

Fig. 8. Craters (left, top view) and crater replicas (right, side view) photographs for the third harmonic of the laser radiation and the three types of the targets: single massive target (**a**), double target with foil (**b**), and double target with disk (**c**).

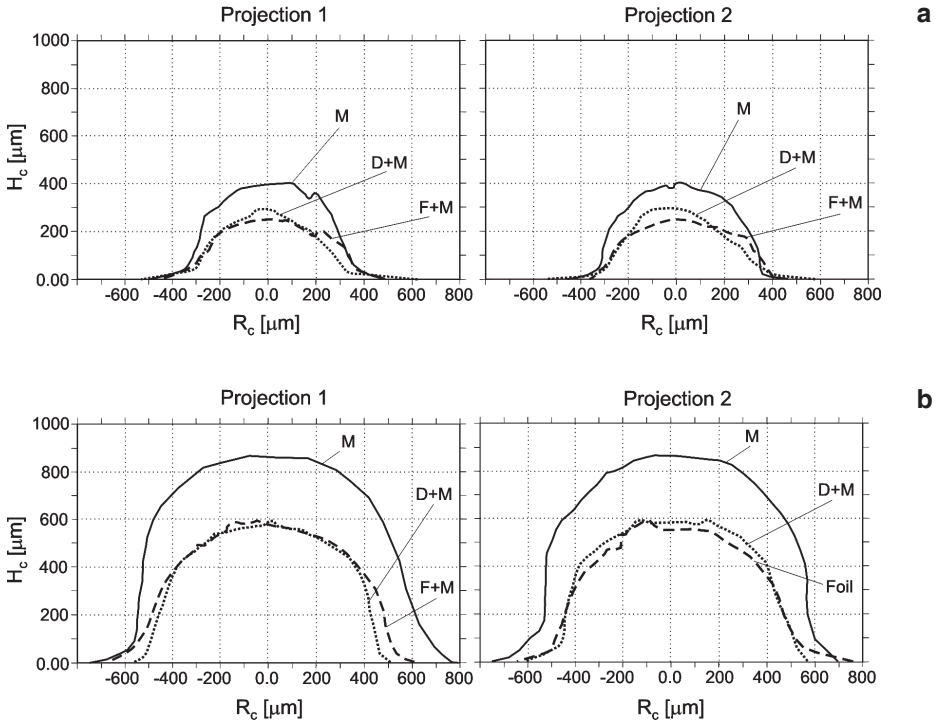

Fig. 9. Crater shapes and dimensions for the first (**a**) and the third (**b**) harmonics of the beam radiation, where: M – single massive target, F+M – double target with foil, and M+D – double target with disk.

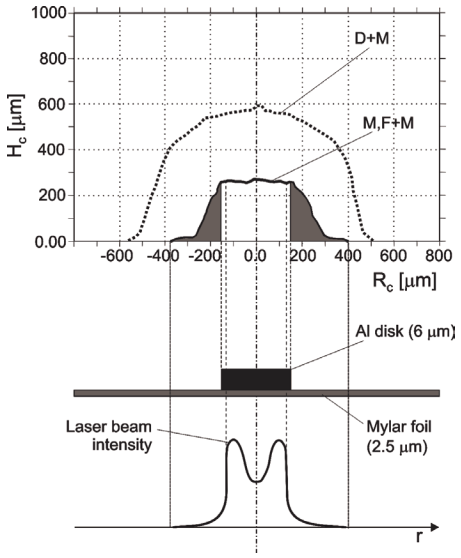

Fig. 10. Illustration of the mylar foil participation in the crater creation by the disk. Notations: D+M – double target with disk, and MF+M – double target with mylar foil only (without disk).

T a b l e. Set of the volumes of craters (in cm^3) for the three types of the targets.

	Single massive target	Double targets	
		Foil + massive target	Disk + massive target
1st harmonic	1.03×10^{-4}	0.64×10^{-4}	0.62×10^{-4}
3rd harmonic	7.46×10^{-4}	3.31×10^{-4}	3.05×10^{-4}

This table clearly shows that for the same harmonics the differences in the volumes of craters between the two types of double targets are relatively small, whereas much more noticeable differences between the volumes of craters are observed in the case of different harmonics. For the massive targets the crater volumes created by the third harmonic are about 7.2 times larger than those created by the first one. In the case of the double targets, the volumes of craters for the third harmonic are about 5 times larger than those for the first one. Differences in efficiencies of the creation of craters by means of the foil fragments and disks with respect to the creation of craters by the direct laser beam action amount to 60% and 40–45% for the first and the third harmonic, respectively.

Finally, we would like to make some notes about our tests concerning the possibility of participation of the holding mylar foil in the crater creation by the disk. Since in this case the mylar foil was not covered by the Al foil (see Fig. 2**b**), the outer part of the mylar foil was accelerated as well and could participate in the crater creation together with the disk itself. To estimate this unwanted effect, one laser shot was fired onto the double target with the disk removed using the third harmonic. The crater obtained by this mylar foil only impact and, for comparison, the crater generated by the disk, are shown in Fig. 10. As can be seen in this figure, participation of the outer part of the laser beam beyond the disk in the crater creation is quite negligible (grey fields on the cross-section of the mylar foil impact crater). Of course, assumption of independent participation of the holding mylar foil in the crater creation in the presence of the disk is not entirely correct. A relatively weak shock wave generated by the mylar foil located outside of the disk is within the reach of the main, much stronger shock wave generated by the disk, so in such a case only a minor amplification of the main shock wave occurs. Thus this method of the determination of the holding mylar foil participation in the crater creation can provide only a very limited piece of information.

5. Discussion of the experimental results

At the beginning we would like to discuss the problem of the direct crater creation by means of the laser beam. The crater volume depends on a fraction of the laser beam energy E_L which is transferred to the shock wave. The process of the laser energy transfer consists of two stages. The first one concerns the laser radiation absorption E_{ab} by an evaporated part of the target. The efficiency of this absorption is expressed by the ratio $K_{ab} = E_{ab}/E_L$. The second one is connected with a transfer of the ablative plasma energy into the shock wave propagating into a non-evaporated solid part of the

target. The ratio of the shock wave energy E_{sw} and the laser radiation absorption E_{ab} is the ablation loading efficiency $\sigma = E_{sw}/E_{ab}$ [8]. Hence, the crater volume V_{cr} is proportional to the product of these two efficiencies, $V_{cr} \propto K_{ab}\sigma E_L$ [9].

As was shown in [9], in the case of the classical inverse bremsstrahlung, the absorption of the laser radiation taking place in the region of the critical plasma density ρ_{cr} and the ablation loading efficiency σ are given by:

$$\sigma = \frac{\sigma_1}{1 + 0.65\dfrac{\xi}{R_L}}, \tag{2}$$

$$\sigma_1 = \frac{0.94}{(\gamma_S + 1)^{1/2}}\left(\frac{\rho_{cr}}{\rho_0}\right)^{1/2}, \tag{3}$$

$$\rho_{cr} = 1.83 \times 10^{-3}\frac{A}{Z\lambda^2} \tag{4}$$

where: ρ_0 – solid state density, R_L – radius of laser beam focal spot, λ – wavelength of the laser radiation, A – atomic weight of the plasma ions, Z – average degree of ionization of the plasma ions, γ_s – the adiabatic index in the condensed matter (γ_s = 5/2 for Al), ξ – size of the plasma torch given by

$$\xi = 1.2\left(\frac{K_{ab}I}{\rho_{cr}}\right)^{1/3}\tau \tag{5}$$

while I denotes laser radiation intensity, τ – laser pulse duration.

The dependence of ablation loading efficiency on the laser radiation wavelength consists of two components. The first one is expressed by a proportion $\sigma \propto \rho_{cr}^{1/2} \propto \lambda^{-1}$. This strong dependence is connected with an increase of the plasma torch density on the solid target–plasma boundary when the laser radiation wavelength decreases. The second component of the growth of ablation loading efficiency σ with a decrease of wavelength λ results from a weakening role of the two dimensional plasma torch expansion. According to Eq. (5) $\xi \propto \rho_{cr}^{-1/3} \propto \lambda^{2/3}$ and the factor of the ablative loading efficiency decreasing due to two dimensional expansion, decreases when the wavelength increases. On the basis of the well known results it is obvious that at the inverse bremsstrahlung absorption the mass of the plasma torch m increases when the laser wavelength decreases, but, on the contrary, its velocity v_{cr} (and temperature T) decreases when laser radiation decreases. These relations are expressed by the formulas [12]:

$$m = \rho_{cr} v_{cr} \tau = \rho_{cr} \left(\frac{K_{ab} I}{\rho_{cr}} \right)^{1/3} \tau \propto \frac{\left(K_{ab} I \right)^{1/3}}{\lambda^{4/3}}, \tag{6}$$

$$T^{1/2} \propto v_{cr} = \left[\frac{2(\gamma - 1)}{3\gamma - 1} \right]^{1/3} \left(\frac{K_{ab} I}{\rho_{cr}} \right)^{1/3} \propto K_{ab}^{1/3} I^{1/3} \lambda^{2/3} \tag{7}$$

where γ denotes the adiabatic index in the plasma torch.

So, it means that in the case of the third harmonic the laser radiation is absorbed in a denser plasma region in comparison with that for the first one (see formula (4)). Thus the mass of the expanding plasma in the case of the third harmonic is larger (see formula (6)), but its temperature and, of course, its expansion velocity, are smaller, since $\xi \propto v_{cr} \propto \lambda^{2/3}$ (see formula (7)).

The results calculated using formulas (2)–(5) have shown that the ablation efficiency in the case of the third harmonic is 5 times greater than that for the first harmonic. Meanwhile, this efficiency, determined on the basis of the experimental data, is 7.2 times greater. Taking into account the crater volume $V_c \propto K_{ab} \sigma E_L$, the ratio of the crater volumes for the third and the first harmonic is given by:

$$\frac{V_{c_3}}{V_{c_1}} = \frac{\sigma_3}{\sigma_1} \frac{K_{ab3}}{K_{ab1}}. \tag{8}$$

Because the experimental data give this ratio equal to 7.2, while from the theoretical calculation $\sigma_3/\sigma_1 = 5$, well now $K_{ab3}/K_{ab1} = 7.2/5 = 1.4$. This estimation allows us to conclude that in the case of the third harmonic the absorption efficiency of the laser radiation is higher than that for the first harmonic by the factor of 1.4.

The important conclusion can be drawn from the comparison of the crater volumes in the case of the double targets. The efficiency of the energy transfer during the non-elastic impact of the accelerated macroparticle with the wall in rest β (the fraction of the macroparticle energy transferred to the wall) depends on the relation between the densities of the macroparticle ρ_p and the wall ρ_w as well as the adiabatic indexes of both materials. According to the calculation in [13], for the same densities of colliding elements ($\rho_p = \rho_w$) and the adiabatic index $\gamma_s = 5/2$ for Al, the efficiency of the macroparticle energy transfer $\beta = 0.58$. This value is in a good agreement with the experimental value of the relative efficiency of the crater creation by means of the macroparticles with respect to that in the case of direct laser beam action for the first harmonic, which amounts to about 60%.

This agreement of the theoretical and experimental results testifies that both the foil fragment and the disk conserve their compact form and the initial Al density until

their collision with the massive part of the target. In the case of the third harmonic the above mentioned relative efficiency of the crater creation is equal to 0.4–0.45. This lower efficiency allows us to conclude that in this case macroparticles undergo decomposition and they have their density at the impact moment smaller than the value of the initial Al density in solid state.

The considerably lower relative efficiency of the energy transfer to the massive part of the target at the collision moment in the case of the third harmonic results from the much larger energy of the shock wave propagating in the macroparticles in comparison with the case of the first harmonic. It is in agreement with the experimental results for the massive targets and the theoretical prediction of a strong growth of ablation loading efficiency with a decreasing laser radiation wavelength. Indeed, when the laser radiation of the third harmonic acts, the shock wave energy and, in consequence, the temperature of the macroparticles (both foil and disk) are several times higher than those for the first harmonic. Therefore, the decomposition of the macroparticles before collision in the third harmonic case runs considerable faster.

Macroparticle velocity to an order of magnitude is equal to the velocity of the shock wave which is proportional to the ablation pressure of plasma torch $v_{sw} \propto (P_a/\rho_0)^{1/2}$, where $P_a \propto \rho_{cr} v_{cr}^2$. So, it is simple to obtain from Eq. (7) that the macroparticle velocity $u \propto K_{ab}^{1/3} \lambda^{1/3}$. Taking into account that the absorption efficiency of the third harmonic laser radiation is higher than that for the first harmonic by the factor of 1.4 we can easily ascertain that the macroparticle velocities in the case of the third harmonic should be higher by the factor of 1.6 than that in the case of the first harmonic. Such simple estimations qualitatively explain the experimental results of the macroparticle velocities determined by the interferometric measurements.

Moreover, because the ratio of the crater volumes for the third and the first harmonic is equal to about 5, assuming the same masses of the macroparticles for both wavelengths, the ratio of the velocities of macroparticles should be equal to the square root of 5 (*i.e.*, ≈ 2.24). Taking into account that the relative efficiency of the crater creation for the third harmonic is about 25% smaller in comparison with that for the first one, the velocities of the particles in the case of the third harmonic should be close to the upper limit of the experimentally determined velocity range.

The conclusion, resulting from the linear electron density diagrams, where the electron number in the vicinity of the target appears smaller in the case of the third harmonic in comparison with the first harmonic case, can be explained in the following way. From the above discussion the temperature of the plasma torch $T \propto \lambda^{4/3}$ (see formula (7)). In our experimental conditions the ratio of the wavelengths of the first and the third harmonic equals 3, so the plasma temperature for the first harmonic is 4.33 times higher. As the interferometric measurements provide the electron density and the amount of free electrons in the plasma stream, the plasma temperature is a very important parameter from the point of view of the ionization degree. The higher ionization degree in the case of the first harmonic means the higher free electron

number. Hence, one gets the higher linear electron density in the vicinity of the target for the case of the first harmonic.

Differences in the $n_e(r, z)$ distributions related to the first and the third harmonic are connected with some properties of the PALS iodine laser beam. In comparison with a solid laser, the iodine laser, having its active medium in a gaseous form, has a more non-uniform distribution of the intensity across the cross-section of the laser beam. In the case of the low output laser energy, below 180 J, the intensity distribution has approximately a flat character along the radius. For higher output laser energy the laser amplifiers cause a decrease in the center of this distribution, the depth of which increases with increasing laser energy. This situation concerns only the first harmonic of the laser radiation. In the case of the third harmonic, to have any laser energy, the output laser energy should be 2–3 times larger, mainly due to the wavelength transformation efficiency which is in the range of 30–50%. The concave character of the intensity distribution is even more pronounced in the case of the third harmonic because of the nonlinear transformation of the DKDP crystal.

Similarity of the character of the plasma expansion for all the targets tested in the case of the first harmonic is connected with the flat intensity distribution of the laser radiation. This homogeneous irradiation of the double targets allows the flat form of the foil (and disk) to be conserved and the plasma expansion can be realized analogously to that for the single massive target.

In the case of the third harmonic, the outer forms of the plasma streams for all the targets are similar. One can assume that the initial conditions of the plasma emission were similar, too. However, differences concern the inner dense plasma which is emitted a bit later. The elongated shape of the dense plasma in the case of the massive target is specific for the annular irradiation of the flat target [14]. Even if the irradiation conditions for both types of double targets were the same as in the previous case, the shape of the dense plasma is essentially distinct. This difference can be only explained by the foil target deformation during the laser action. This deformation should have a ring like form, in accordance with the laser beam radiation intensity distribution. Reconstruction of plasma emission from target surface thus deformed is in a good agreement with the actual electron density distribution.

Even if the target material evaporation and plasma ablation processes last a very short time (during the laser beam action), expansion of the ablative plasma lasts a relatively long time (longer than the period of our interferometric observation).

The growth of the electron density in the vicinity of the single massive target at the time of 8 ns after the laser action for both harmonics can testify to the appearance of a new plasma source. This source can only be connected with the crater creation. At this time the accelerated macroparticles run away far from their initial positions and such growth in the double targets case does not appear.

Our expectation concerning higher efficiency of the disk, in comparison with the foil, in the process of the crater creation has not been fulfilled. The efficiencies of

both methods under our experimental conditions are comparable. For the same wavelength of the laser radiation both the velocities of the two kinds of the macroparticles and the volumes of the craters generated by them are approximately the same. Thus one can come to the conclusion that the kinetic energies of these macroparticles and, going even further, their respective masses as well, are the same. Because the macroparticle mass is connected with its diameter, one can assume that the extracted foil fragment diameter is approximately equal to that of the disk. This conclusion is confirmed by the similar shapes of the craters for the both kinds of macroparticles.

6. Conclusions

Our investigations have shown a very useful role of the interferometric method for visualization of the laser produced plasma expansion and determination of the dynamics of the plasma and the accelerated macroparticles. This active plasma diagnostic method, although rather complex (both technically and methodologically), is irreplaceable in such experiments.

On the other hand, the relatively simple replica method for measuring the crater parameters also provides many interesting and important information about interaction of the laser beam or macroparticles with a massive target. Both these methods give evidence about the processes of laser energy transformation into the energy of the shock wave in solids, energy transfer from a laser-driven accelerated macroparticle to the massive target, and even the absorption efficiency of the laser radiation in plasmas. Combination of these diagnostic methods allows obtaining a nearly full picture of the processes analyzed.

Acknowledgments – The work was supported in part by the "Access" EU programme (contract HPRI-CT--1999-0053), by the Russian Foundation of Basic Research (Project 02-02-16966), IAEA (Res.Proj. 11655/RBF) and INTAS (Proj. 01-0572), the Czech participation by MSMT CR (Proj. LN00A100), PALS operation by AS CR (Grant K2043105).

References

[1] RIPIN B.H., DECOSTE R., OBENSCHAIN S.P., BODNER S.E., MCLEAN E.A., YOUNG F.C., WHITLOCK R.R., ARMSTRONG C.M., GRUN J., STAMPER J.A., GOLD S.H., NAGEL D.J., LEHMBERG R.H., MCMAHON J.M., Phys. Fluids **23** (1980), 1012.

[2] GRUN J., OBENSCHAIN S.P., RIPIN B.H., WHITLOCK R.R., MCLEAN E.A., GARDNER J., HERBST M.J., STAMPER J.A., Phys. Fluids **26** (1983), 588.

[3] EIDMANN K., AMIRANOFF F., FEDOSEJEVS R., MAASWINKEL A.G.M., PETSCH R., SIGEL R., SPINDLER G., YUNG-LU TENG, TSAKIRIS G., WITKOWSKI S., Phys. Rev. A **30** (1984), 2568.

[4] GUS'KOV S.YU., Quantum Electron. **31** (2001), 885.

[5] BASOV N.G., GUS'KOV S.YU., FEOKISTOV L.P., J. Sov. Laser Res. **13** (1992), 396.

[6] TABAK M., HAMMER J., GLINSKY M.E., KRUER W.L., WILKS S.C., WOODWORTH J., CAMPBELL E.M., PERRY M.D., MASON R.J., Phys. Plasmas **1** (1994), 1626.

[7] GUS'KOV S.YU., ZVEREV V.V., ROZANOV V.B., Quantum Electronics **13** (1983), 498.

[8] GUS'KOV K.S., GUS'KOV S.YU., Quantum Electronics **31** (2001), 305.
[9] DOSKACH I.Y., GUS'KOV S.Y., JUNGWIRTH K., KALAL M., KASPERCZUK A., KRALIKOVA B., KROUSKY E., LIMPOUCH J., MASEK K., PFEIFER M., PISARCZYK T., ROHLENA K., ROZANOV V.B., SKALA J., ULLSCHMIED J., Proc. SPIE **5228** (2003), 121.
[10] JUNGWIRTH K., CEJNAROVA A., JUHA L., KRALIKOVA B., KRASA J., KROUSKY E., KRUPICKOVA P., LASKA L., MASEK K., MOCEK T., PFEIFER M., PRAG A., RENNER O., ROHLENA K., RUS B., SKALA J., STRAKA P., ULLSCHMIED J., Phys. Plasmas **8** (2001), 2495.
[11] KASPERCZUK A., PISARCZYK T., Opt. Appl. **31** (2001), 63.
[12] AFANAS'EV YU.V., GUS'KOV S.YU., *Energy transfer to the plasma in laser target*, [In] *Nuclear Fusion by Inertial Confinement*, [Ed.] G. Velarde *et al.*, CRC PRESS, Ann Arbor, 1993, pp. 99–118.
[13] GUS'KOV S.YU., Proc. SPIE **5228** (2003), 221.
[14] BORODZIUK S., KASPERCZUK A., PISARCZYK T., GUS'KOV S., ULLSCHMIED J., KRALIKOVA B., ROHLENA K., SKALA J., KALAL M., PISARCZYK P., Opt. Appl. **34** (2004), 31.

Received April 28, 2004
in revised form July 7, 2004